Published in final edited form as:

Biomaterials. 2012 September ; 33(27): 6305–6312. doi:10.1016/j.biomaterials.2012.05.053.

The effect of nitric oxide surface flux on the foreign body response to subcutaneous implants

Scott P. Nichols[a], **Ahyeon Koh**[a], **Nga L. Brown**[b], **Michael B. Rose**[b], **Bin Sun**[a], **Danielle L. Slomberg**[a], **Daniel A. Riccio**[a], **Bruce Klitzman**[b], and **Mark H. Schoenfisch**[a,*]

Mark H. Schoenfisch: schoenfisch@unc.edu

[a]Department of Chemistry, University of North Carolina at Chapel Hill, Chapel Hill, NC 27599, USA

[b]Kenan Plastic Surgery Research Laboratories, Department of Biomedical Engineering, Duke University Medical Center, Durham, NC 27710, USA

Abstract

Although the release of nitric oxide (NO) from biomaterials has been shown to reduce the foreign body response (FBR), the optimal NO release kinetics and doses remain unknown. Herein, polyurethane-coated wire substrates with varying NO release properties were implanted into porcine subcutaneous tissue for 3, 7, 21 and 42 d. Histological analysis revealed that materials with short NO release durations (i.e., 24 h) were insufficient to reduce the collagen capsule thickness at 3 and 6 weeks, whereas implants with longer release durations (i.e., 3 and 14 d) and greater NO payloads significantly reduced the collagen encapsulation at both 3 and 6 weeks. The acute inflammatory response was mitigated most notably by systems with the longest duration and greatest dose of NO release, supporting the notion that these properties are most critical in circumventing the FBR for subcutaneous biomedical applications (e.g., glucose sensors).

Keywords

Nitric oxide release; Foreign body response; Inflammation; Biocompatibility; Polyurethane

1. Introduction

The foreign body response (FBR) is a major impediment toward the development and long-term functionality of most implanted biomedical devices. Implantation disrupts the native tissue, initiating the FBR with the adhesion of proteins and other biomolecules to the device surface [1,2]. This process continues with the infiltration of inflammatory cells that attempt to phagocytose the foreign object [1,2]. Within a few weeks, the cells create a relatively avascular collagen-rich encapsulation, effectively sequestering the implant from the surrounding tissue [3]. Macrophages undergo cell fusion to form multi-nucleated foreign body giant cells (FBGCs) that remain at the implant surface and enhance its degradation, often leading to device failure or performance mitigation [4,5]. In the case of implanted glucose sensors, this isolation blocks the diffusion of glucose from surrounding tissue, inhibiting accurate measurements.

*Corresponding author. Tel.: +1 919 843 8714; fax: +1 919 962 2388.

Appendix A. Supplementary material: Supplementary material associated with this article can be found, in the online version, at http://dx.doi.org/10.1016/j.biomaterials.2012.05.053.

Efforts to improve the fate of subcutaneous implants have largely focused on developing materials with chemical and physical properties that mitigate the FBR and allow better tissue integration. The use of natural materials (e.g., collagen [6,7]) and synthetic polymers [8,9] to alter the tissue – sensor interface has slightly improved tissue integration of such devices. However, complete avoidance of the FBR has yet to be achieved and the field of biomaterials has evolved to include the design of coatings that actively release FBR mediators [10]. For glucose sensors, the focus has been on materials that release anti-inflammatory (i.e., dexamethasone) and/or pro-angiogenic (i.e., vascular endothelial growth factor (VEGF)) mediators [11–14]. Unfortunately, reports on the combined use of dexamethasone and VEGF have been controversial, possibly due to the molecules acting in an antagonistic manner [13–16].

Other work has focused on the design of interfaces that release nitric oxide (NO), an endogenous signaling molecule that plays multiple roles in the immune response including cytokine production [17,18], collagen deposition [19–22], angiogenesis [23], and anti-microbial activity [24]. Hetrick et al. [25] examined the subcutaneous in vivo response to NO-releasing *N*-diazeniumdiolated xerogels coated onto rectangular silicone rubber substrates. These coatings released ~1.35 μmol/cm^2 of NO over 72 h with 50% m of the NO payload exhausted within 5 h. A >50% decrease in collagen capsule thickness was observed after 3 weeks of implantation [25]. Furthermore, NO release reduced the chronic inflammation at 3 and 6 weeks while enhancing angiogenesis adjacent to the implant after only 1 week of implantation [25]. In a separate study, mitigation of the FBR with NO release was evaluated by quantifying glucose diffusion to NO-releasing microdialysis probes in rat subcutaneous tissue [26]. In this case, 4.6 μmol NO/cm^2 was released each day by perfusing saturated NO solutions for 8 h over 14 d of implantation [26]. The NO at the tissue—probe interface resulted in enhanced glucose diffusion into the NO-releasing probe after 7 d compared to controls, an effect that would effectively decrease implantable glucose sensor lag time [26]. Histological analysis at 14 d revealed a thinner collagen capsule and reduced inflammatory response for the NO-releasing probes [26]. Gifford et al. [27] prepared subcutaneous glucose sensors capable of releasing NO for 18 h by doping the NO donor (Z)-1-[N-methyl-N-[6-(N-butylammoniohexyl)amino]]-diazen-1-ium-1,2-diolate (DBHD/N_2O_2) into a polymer matrix. The in vivo inflammatory response was significantly reduced in response to the NO-releasing materials after implantation of 24 h but not at 48 h [27]. The authors noted that the reduction in the inflammatory response correlated well with the NO release duration, supporting a need for long-term NO release [27]. Decreased collagen encapsulation and inflammation with increased angiogenesis have been identified previously as key factors that enhance glucose sensor function [28]. Taken together, these reports support the promise of improved tissue integration and subcutaneous sensor functionality using materials that release NO.

While the positive effects of NO are well known, the optimal rate and amounts of NO release are unclear. Previously, Koh et al. [29] reported the ability to dope NO-releasing nanoparticles of various compositions into polyurethane (PU) matrices and control the NO release kinetics based on the properties of the PU and/or NO-releasing scaffold. The NO-releasing properties from these materials suggest that they are ideal for systematically studying the effect of NO on the FBR from chemically identical interfaces. To better mimic the human FBR and wound healing, this study was carried out in a porcine subcutaneous implant model [30].

2. Methods and materials

Tetramethoxysilane (TMOS) and L-proline were purchased from Sigma Aldrich (St. Louis, MO). 3-Mercaptopropyltrimethoxysilane (MPTMS), N-(2-aminoethyl)-3-

aminopropyltrimethoxysilane (AEAP3), and tetraethoxysilane (TEOS) were purchased from Gelest (Tullytown, PA). Diethylenetriamine pentaacetic acid (DTPA) was purchased from Fluka (Buchs, Switzerland). Ethanol (EtOH), methanol (MeOH), tetrahydrofuran (THF), and ammonia solution (NH_4OH, 30 wt% in water) were purchased from Fisher Scientific (Fair Lawn, NJ). Stainless steel wire (316L, 381 μm diameter) was purchased from McMaster-Carr (Atlanta, GA). Tecoplast TP-470-000 (TP-470), Tecophilic HP-93A-100 (HP 93A) and Tecoflex SG-80A (TPU) were gifts from Thermedics (Woburn, MA). Hydrothane AL 25-80A (HPU) was a gift from AdvanSource Biomaterials Corporation (Wilmington, MA). Nitric oxide was purchased from Praxair (Danbury, CT). Nitric oxide calibration gas (26.39 ppm; balance nitrogen), nitrogen, and argon were purchased from National Welders (Raleigh, NC). Distilled water was purified to 18.2 MΩ/cm with a Millipore Milli-Q Gradient A-10 water purification system (Bedford, MA). All other reagents were reagent grade and used as received.

2.1. Preparation of NO-releasing scaffolds

1-[2-(Carboxylato)pyrrolidin-1-yl]diazen-1-ium-1,2-diolate (PROLI/NO) was prepared by converting the secondary amine in L-proline to an *N*-diazeniumdiolate following a previously described procedure [31]. Nitric oxide-releasing silica particles were synthesized based on the sol-gel process via the co-condensation of AEAP3 (70 mol% balance TMOS) or MPTMS (75 mol% balance TEOS) [32,33]. Subsequent *N*-diazeniumdiolation of the amine-containing particles was performed under high pressure of NO for 3 d in the presence of sodium methoxide in methanol at room temperature [32]. Nitrosation of the thiol-containing nanoparticles was carried out by reaction with acidified nitrite in the dark at 0 °C [33]. The details of the NO-releasing characteristics for each system are provided in supporting information (Table S1).

2.2. Preparation of polyurethane-coated wire substrates

Stainless steel wires were cut to ~5 cm and cleaned by sonicating sequentially in EtOH, water, and EtOH again for 30 min each and sterilized by autoclaving. To create the NO-releasing coating, the NO-releasing vehicle (i.e., PROLI/NO, AEAP3 nanoparticles or MPTMS nanoparticles) was dispersed into cold EtOH (2.5 mL) at concentrations of 36 or 72 mg/mL. This solution was then mixed with an equal volume of 50:50 wt% HPU/TPU (160 mg/mL total PU) dissolved in THF (2.5 mL) for a resulting concentration of 18 or 36 mg/mL scaffold and 80 mg/mL PU in 50:50 v% EtOH/THF. In a sterile laminar flow hood, wires were then dip-coated four times in the scaffold-containing PU solution with brief ambient drying between dips. A polyurethane topcoat (TP-470, TPU, HPU/TPU, HPU or HP 93A; 40 mg/mL dissolved in THF) was then applied and allowed to dry. The PU-coated wire was then cut to 3 cm, and the freshly cut end was coated with the same PU topcoat. The PU-modified wires were placed into individual, sterile, microcentrifuge tubes and kept vacuum sealed in the dark at −20 °C until use. Control (non-NO-releasing) wires were made using the same protocol but with no scaffold in the PU solutions.

2.3. Characterization of polyurethane-coated wires

Scanning electron microscopy was used to evaluate the macroscopic surface roughness of the coated wires using a Quanta 200 (FEI, Hillsboro, OR) in high vacuum mode before and after the topcoating process. Release of NO was measured continuously using a Sievers 280i Chemiluminescence Nitric Oxide Analyzer (NOA) (Boulder, CO) [34]. Calibration of the NOA was performed with both air passed through a Sievers NO zero filter and 26.39 ppm NO gas (balance N2). For analysis, NO-releasing wire substrates were immersed in 25 mL of deoxygenated phosphate buffered saline (PBS; 10 m_M, pH 7.4). Released NO was carried to the analyzer in a nitrogen stream (200 mL min^{-1}). Temperature control was maintained using a water bath at 37 °C. Nitric oxide release from nitrosothiol nanoparticle-doped

coatings were studied by shielding the sample flask from light and using PBS with 500 μM DTPA to chelate trace copper. The thickness of the wire coatings was estimated by optical microscopy.

2.4. Silicon elemental analysis

To characterize particle stability (via leaching) in the various polyurethane polymers, substrates were incubated at 37 °C in PBS (1 mL) for 1, 3 and 6 weeks. Samples were then further prepared for Si elemental analysis by adding aqua regia (2.5 mL), hydrofluoric acid (1 mL), and 40% triethanolamine (3.575 mL) to dissolve the particles, and then diluted to 50 mL with water. To determine the mass of silica nanoparticles contained in the PU films, the coatings were dissolved in piranha solution (1 mL), exposed to hydrofluoric acid (1 mL) and 40% triethanolamine (3.575 mL), then diluted to 50 mL with water. (CAUTION: hydrofluoric acid and piranha are extremely corrosive and require special handling). The silicon concentration in the solutions was subsequently measured using inductively coupled plasma-optical emission spectroscopy (ICP-OES; Prodigy, Teledyne Leeman Labs, Hudson, NH).

2.5. Implantation and explantation of wire substrates

The animal protocol used in this study was reviewed and approved by the IACUC at Duke University. Coated wire substrates were implanted into seventeen mixed breed Yorkshire-type piglets weighing approximately 5–7 kg. Pigs were initially anesthetized with ketamine:xylazine (20 mg/kg and 2 mg/kg, respectively) and maintained on 2–4% isoflurane (v/v in O_2) during implantation. The dorsal skin was prepared by clipping of the hair and triplicate scrubbing with chlorhexidine and alcohol. Four 1 cm incisions were created 4 cm lateral to the dorsal midline and 8 cm and 18 cm caudal to the scapulae using a scalpel. Five or six wires were then inserted radially (“clock hour” pattern) in the 2,4,6,8,10, and 12 o'clock positions, extending 2 cm out from the incision. The 6 o'clock position was eliminated in two caudal implant sites, resulting in 22 wires implanted per pig.

After 3,7,21 or 42 d, pigs were anesthetized and the tissue surrounding the wire implants was explanted and placed into 10% buffered formalin (v/v) for 24 h, then transferred to 70% EtOH (v/v in H2O) for at least 24 h prior to embedding into paraffin. Sections of the paraffin embedded tissue were stained with Masson's trichrome or hematoxylin and eosin (H&E). Micrographs of the trichrome and H&E stained samples were collected using 4,10, and 20× objectives on a Nikon Eclipse TE2000-U with a Nikon Digital Sight DS-2Mv digital camera (Nikon Inc., Melville, NY).

2.6. Histological analysis

Histological analysis was performed on all explanted tissue samples. Capsule thickness was measured from Masson's trichrome-stained tissue sections. The foreign body capsule was defined as beginning at the edge of the implant and consisting of the region of dense collagen oriented parallel to the implant. The end of the capsule thickness was determined to be where collagen was no longer the primary tissue constituent (indicated by a decrease in the density of blue—green stain) nor oriented parallel to the surface. Eight capsule thickness measurements taken radially at 45° intervals were averaged for each image. Three images of the collagen capsule were processed using a previously developed MATLAB (The MathWorks, Natick, MA) program that quantifies the percent collagen [35,36]. The program defines collagen from trichrome-stained images by the characteristic blue—green color, divides the number of collagen positive pixels by the total pixels in the image, and multiplies this ratio by 100 to obtain percent collagen. Hematoxylin and eosin-stained tissue sections were used to measure the inflammatory response. The inflammatory response, as determined by cell density, was determined by counting all cell nuclei within 50 μm of the

implant surface from three 50 × 100 μm^2 fields from each slide. Cell nuclei were defined as the purple-stained, spherical features in the H&E-stained tissue sections. Histology data are expressed as mean ± standard error of the mean and tested for significance (i.e., $p < 0.05$) using a non-parametric Wilcoxon rank-sum test.

3. Results and discussion

3.1. Characterization of polyurethane coatings

Wire substrates were successfully coated with particle-doped polyurethanes (PUs) capable of releasing NO via dip-coating. The use of wire substrates was pursued to mimic the shape and size of an electrochemical glucose sensor. Both size and shape have been shown to affect the FBR [37,38]. The thickness of the PU coatings remained constant even with the incorporation of a range of NO-releasing scaffolds and concentrations. For example, control PU and 36 mg/mL MPTMS nanoparticle-doped PU coatings were 46 ± 4 and 49 ± 4 μm, respectively. Prior to topcoating, the particle-doped films exhibited markedly greater surface roughness than controls as evaluated using SEM (Fig. 1A). As previous in vivo studies have reported that surface roughness may significantly alter the FBR [39,40], a PU topcoat was added (Fig. 1B) to ensure that the tissue response observed in vivo was a result of NO release and not physical properties.

Although silica is generally considered non-toxic [41], leaching of nanoparticles was quantified to address concerns of unexpected effects in vivo. To determine the percentage of silica particles leached, the mass of nanoparticles within the films was measured by dissolving the PU coatings and quantifying via ICP-OES. Wires dipcoated in 36 mg/mL AEAP3 nanoparticle-doped PU and 36 mg/mL MPTMS nanoparticle-doped PU contained 1.11 ± 0.19 mg and 1.24 ± 0.13 mg of silica nanoparticles, respectively. Over 6 weeks, AEAP3 nanoparticles leached 4.2 ± 0.7% of the total loaded scaffold, with the majority of the leaching (>90%) occurring during the first 3 weeks. The MPTMS soak solutions had no detectable leaching, likely due to the larger particle size of the MPTMS (~ 750—900 nm) compared to the AEAP3 (~ 110–150 nm) nanoparticles.

3.2. Nitric oxide release from polyurethane films

To evaluate the effect of NO release kinetics on the FBR, several NO-releasing scaffolds were employed including PROLI/NO, AEAP3 nanoparticles, and MPTMS nanoparticles. The low molecular weight (LMW) N-diazeniumdiolate PROLI/NO provided the fastest NO release with >90% of NO storage liberated after 6 min. Longer durations of NO release from *N*-diazeniumdiolate donors was achieved using a hybrid silica nanoparticle scaffold containing AEAP3 exhibiting a NO-release half-life of 185 min. By varying the water uptake by selection of the PU topcoat, NO release kinetics were further tuned for *N*-diazeniumdiolate systems whereby NO donor composition is proton initiated [42,43]. As shown in Table 1, the four PUs used in the study were chosen in part due to their water uptake [29].

The release of NO from *N*-diazeniumdiolate and *S*-nitrosothiol NO donors follows pseudo first-order kinetics. Although doping the NO donors into polyurethane matrices may slow NO donor breakdown (and thus NO release), the materials still follow approximate first-order kinetics, with an initial maximum and exponential decay in NO flux. Due to rapid NO donor breakdown, LMW PROLI/NO-doped PUs released NO rapidly (~24 h) and with the greatest NO fluxes (1436—3128 pmol cm^{-2} s^{-1}) depending on the polyurethane matrix (Table 2). The prominent burst of NO may impact the FBR. For example, exogenous NO has been shown to inhibit platelet adhesion and aggregation, and thus elevated NO may slow early healing [44,45]. Compared to the PROLI/NO-doped polymers, the NO release from AEAP3 nanoparticle-doped PUs (Tables 3 and 4) was significantly longer in duration (up to

72 h) due to the longer half-life of the AEAP3 nanoparticles. As expected for each of the PROLI/NO and AEAP3 systems, the total NO payload for any given scaffold and concentration was the same regardless of topcoat.

In contrast to the *N*-diazeniumdiolate-based scaffolds, *S*-nitrosothiols decompose when exposed to heat, light, or Cu^{+} to form 1 mol of NO per mol of thiol [46]. Furthermore, the decomposition of *S*-nitrosothiols is not affected by water uptake and therefore only the HPU/TPU polyurethane topcoat was utilized for MPTMS nanoparticle-doped PUs. While the MPTMS nanoparticles have similar initial release kinetics as the *N*-diazeniumdiolate systems, the *S*-nitrosothiol nanoparticles release lower levels of NO over long periods through thermal release mechanisms. As expected, the MPTMS nanoparticle-doped PUs released NO for the longest duration, with NO still detectable at 14 d (Table 5). Of note, previously implanted NO release studies are based on materials capable of uninterrupted NO release for up to 3 d [25,27]. The 36 mg/mL MPTMS nanoparticle-doped PUs produced the highest NO payload (9.3 (μmol cm^{-2}) in this study, ~7 times more NO than previous subcutaneous NO-releasing xerogels [25]. Based on the nanoparticle concentrations measured via the ICP-OES leaching study, the predicted total NO release for the 36 mg/mL AEAP3 and MPTMS nanoparticle-doped PUs are 6.3 and 10.1 μmol cm^{-2}, respectively. The slight loss in NO likely occurs during the wire dipcoating process. Moisture, light, and heat that are unavoidable under ambient conditions may initiate NO release from both *N*-diazeniumdiolate- and *S*-nitrosothiol-based scaffolds. The range of NO release kinetics utilized in this study allowed for the investigation of the effects of NO release flux (initial burst versus sustained delivery) to be compared.

3.3. Collagen deposition

A characteristic event of the FBR is collagen encapsulation that begins to form 1–2 weeks after implantation. The capsule persists for the life of the device and has low microvessel density [3,47] impeding diffusion of analytes from the surrounding native tissue and blood capillaries [48]. For glucose sensors, the collagen capsule results in reduced sensitivity and increased lag time [49–52]. Capsule thickness and collagen density via Masson's trichrome-stained histology was thus evaluated as a function of NO release kinetics and doses.

As expected, collagen capsule formation surrounding PU-coated wire substrates was not observed until 3 weeks following implantation. The collagen capsule thickness for all wire substrates after 3 and 6 weeks of implantation are summarized in Fig. 2. At 3 weeks (Fig. 2A), PROLI/NO-doped PUs showed no significant reduction in the collagen capsule thickness relative to control ($p < 0.05$). In contrast, both the TPU and TP-470 PU topcoats significantly reduced collagen capsule formation for both the 18 mg/mL and 36 mg/mL AEAP3 nanoparticle-doped PUs versus controls. Both TPU and TP-470 are characterized by low water uptake and thus enabled the longest NO release for the *N*-diazeniumdiolate particle-doped PU systems. The data from the AEAP3 nanoparticle-doped PUs suggest that longer NO-releasing substrates with similar NO payloads more successfully mitigate the FBR. Furthermore, the data suggests that the total NO payload may be less important than the NO release kinetics for reducing collagen encapsulation at 3 weeks. For example, the TP-470 topcoated 18 mg/mL AEAP3 nanoparticle-doped PU has a lower total NO payload but a greater NO flux at 48 h than HP 93A, HPU or HPU/TPU topcoated 36 mg/mL AEAP3 nanoparticle-doped PUs (Tables 3 and 4). These slow NO release kinetics correlate well with the mitigated FBR. The even longer (in duration) NO-releasing PUs (i.e., MPTMS nanoparticle-doped) reduced the collagen capsule at both dopant concentrations of 18 and 36 mg/mL by ~ 64 and ~ 77%, respectively. Indeed, the MPTMS nanoparticle-doped PU systems represented the two largest decreases in collagen capsule thickness at 3 weeks.

At 6 weeks, the average collagen capsule thickness adjacent to all implanted materials was reduced compared to 3 weeks. While not anticipated, a decrease in collagen encapsulation surrounding subcutaneous materials has been observed over time for non-NO-releasing materials [53]. As was also observed at 3 weeks, PROLI/NO-doped PUs did not appreciably reduce the collagen capsule thickness (Fig. 2B). Of the 18 mg/mL AEAP3 nanoparticle-doped PUs, only the HPU/TPU topcoated system displayed a significant reduction in capsule thickness (~ 59% reduction vs. control). It is currently unknown why this composition would best mitigate the FBR. The other 18 mg/mL AEAP3 nanoparticle-doped PU systems with slightly longer or shorter NO durations proved inadequate in altering the resulting capsule thickness. Although speculative at this stage, we believe that the NO release from the HPU/TPU topcoat provided both a sufficiently high maximum and NO release duration. Other PU topcoats resulted in either insufficient maximum NO flux or duration negatively impacting the FBR mitigation. Clearly other relevant parameters are likely since materials with a greater maximum flux and similar NO flux at 48 h (e.g., HPU topcoated 36 mg/mL AEAP3 nanoparticle-doped PUs) did not result in similar reductions in capsule thickness.

In contrast to the 18 mg/mL AEAP3 nanoparticle-doped PUs, the three longest NO-releasing PU topcoats (i.e., HPU/TPU, TPU, and TP-470) applied to the 36 mg/mL AEAP3 nanoparticle-doped PU systems were capable of significant reductions in the capsule thickness at 6 weeks. The higher incidence of significant capsule thickness reductions with the 36 versus the 18 mg/mL AEAP3 nanoparticle system indicates a possible advantage to materials releasing a greater NO payload. The NO release originating from low water uptake PU topcoats (i.e., HPU/TPU, TPU, and TP-470) provided the longest NO release duration for the 36 mg/mL AEAP3 nanoparticle system albeit with identical NO payloads to the statistically insignificant PU topcoats (i.e., HP 93A and HPU). The data from the 36 mg/mL AEAP3 nanoparticle systems further indicates that NO release kinetics of implanted materials greatly impact the FBR. Both concentrations of the MPTMS nanoparticle-doped polyurethanes significantly reduced the capsule size with the 18 and 36 mg/mL MPTMS nanoparticle systems achieving a ~50 and ~76% reduction in capsule thickness, respectively. Since the long-term NO release fluxes (i.e., 7–14 d) for both the 18 and 36 mg/mL MPTMS nanoparticle systems were similar (Table 5), the difference in the initial 7 d of NO release is attributed to the enhanced FBR mitigation. The combination of significant NO levels initially and sustained, low NO release over 14 d may improve tissue integration by altering the initial inflammatory response as reported by Hetrick et al. [25]. The 36 mg/mL MPTMS nanoparticle-doped systems reduced the collagen encapsulation to the greatest level at both 3 and 6 weeks of implantation, indicating the advantage of a large initial NO payload and sustained NO release for decreasing capsule thickness.

The density of the collagen within the encapsulation is another factor that may affect the sequestering of the foreign body. A previously developed and implemented MATLAB program was thus used to quantify collagen density in captured micrographs of the collagen capsule [36]. The program measures the number of pixels attributed to collagen when stained with Masson's trichrome, divides this number by the total pixels in the image, and multiplies by 100 to give a collagen density index (CDI) ranging from 0 to 100, with a CDI value of 100 indicating every pixel represents collagen. At 3 weeks, the capsules surrounding the HP 93A, HPU, and TPU topcoated PROLI/NO systems exhibited significantly increased CDI compared to controls (Fig. 3A) with no other NO-releasing substrates exhibiting a significant change. Of note, the maximum NO flux from PROLI/NO-doped PUs was an order of magnitude greater (1436—3128 pmol cm^{-2} s^{-1}) than that from any previously implanted NO-releasing materials. Though the NO payload (~4 μmol/cm^2) from the PROLI/NO systems falls between that of the two concentrations of AEAP3 nanoparticle systems, neither concentration of AEAP3 nanoparticle systems exhibited an

increase in CDI at 3 weeks. As such, the CDI enhancement is most likely the result of the large NO bolus from the PROLI/NO systems. The inability to significantly reduce capsule thickness while simultaneously causing an increase in the collagen density indicates long-term disadvantages of bolus NO release from implant surfaces.

At 6 weeks, the capsules surrounding the TP-470 topcoated 36 mg/mL AEAP3 and HPU/TPU topcoated 36 mg/mL MPTMS nanoparticle systems showed significantly increased CDI versus controls (Fig. 3B). This enhancement of collagen density at 6 weeks may also be the result of too much NO. Previously reported microdialysis implants with high NO payloads (4.6 μmol cm^{-2} each day) also increased collagen density [26], perhaps not unexpected since NO has been shown to enhance collagen deposition from fibroblasts [20–22]. Nevertheless, the NO-releasing microdialysis probes resulted in superior glucose recovery compared to control probes despite an enhanced CDI [26]. While the TP-470 topcoated 36 mg/mL AEAP3 and the HPU/TPU topcoated 36 mg/mL MPTMS nanoparticle systems were characterized by increased CDI, both of these materials significantly reduced the thickness of the collagen encapsulation. Therefore, the materials may still be advantageous for certain subcutaneous device applications (e.g., glucose sensors).

3.4. Inflammatory response

The localization of inflammatory cells may contribute to erratic device (e.g., sensor) performance and ultimate failure [54]. Inflammatory cells adjacent to the implant become activated while attempting to phagocytose the foreign body. This activation decreases local pH and produces superoxide and peroxide. Several studies have linked these factors to poor sensor performance [54–56]. As the FBR progresses, the formation of foreign body giant cells (FBGCs) enhances implant degradation, also diminishing the sensor lifetime [4,5]. To quantify the inflammatory response, the number of cell nuclei localized within 50 μm of the implant surface was measured in hematoxylin and eosin-stained histology sections. For these reasons, the inflammatory response to the NO-releasing substrates was examined histologically at both acute (3 and 7 d) and chronic (3 and 6 week) stages.

During the acute phase, the NO release led to a significant reduction in the inflammatory response (Fig. 4A and B). The inflammatory response was most significantly impacted by substrates with large and long NO release (e.g., 36 mg/mL AEAP3 and MPTMS nanoparticle systems). The PROLI/NO and 18 mg/mL AEAP3 nanoparticle systems, only releasing NO up to 48 h, did not decrease the inflammatory response. Likewise, Gifford et al. reported that the inflammatory response only seemed to be influenced (reduced) while NO was actively released [27]. However, the HPU/TPU topcoated 18 mg/mL AEAP3 nanoparticle system was also observed to decrease the inflammatory response, likely due to the achievement of optimal release kinetics and duration via the HPU/TPU topcoat. Of the 36 mg/mL AEAP3 nanoparticle systems, the three topcoats with the slowest NO release kinetics (i.e., HPU/TPU, TPU, and TP-470) also significantly reduced the inflammatory cell density adjacent to the implant. The difference in inflammation with identical NO payloads further stresses the need to extend NO release to achieve the most desirable FBR. At 1 week, only the 36 mg/mL MPTMS nanoparticle system, releasing the greatest NO flux over this length of time, showed a statistically significant reduction in the inflammatory response, further supporting Gif-ford's observations.

In contrast, the chronic inflammatory response was largely unaffected by NO release in this study as no NO-releasing substrate was capable of mitigating the inflammatory response at 3 or 6 weeks of implantation (Fig. 4C and D). At 6 weeks, the 36 mg/mL MPTMS nanoparticle system resulted in an apparent 22% reduction in the inflammatory response ($0.05 < p < 0.10$). Such results are contradictory to a previously reported short-term (72 h) NO-releasing xerogel system that improved the chronic inflammatory response [25], but are

in good agreement with the Gifford et al. study where the inflammatory response was mitigated only during active NO release from the implant [27]. It is important to note previous experiments by Gifford et al. and Hetrick et al. were performed in rodent models that may not be as quantitatively relevant to humans as porcine models [25,27,30].

4. Conclusions

These results stress the need to examine NO release kinetics in the development of implantable materials. Furthermore, there is a need to create materials with NO release durations exceeding two weeks, specifically in relation to mitigating the inflammatory response. Approaches for enhancing NO release durations include increasing the hydrophobicity of the polymer matrixor making use of longer releasing *S*-nitrosothiol NO donors (e.g., tertiary *S*-nitro-sothiols). Of course, such changes may affect glucose sensor response/performance. Although the mitigation of the FBR observed in our study may prove beneficial for indwelling glucose sensors, the effects of NO release should also be evaluated for percutaneous implants to confirm if the same degree of tissue integration is achieved. Studies evaluating the effects of NO release on the performance of percutaneous implants are currently underway in our lab.

Supplementary Material

Refer to Web version on PubMed Central for supplementary material.

Acknowledgments

The authors acknowledge research support from the National Institutes of Health (NIH Grant EB000708). The authors also thank Prof. W. Monty Reichert of the Department of Biomedical Engineering at Duke University for use of the Nikon Eclipse TE2000-U microscope.

References

1. Anderson JM, Rodriguez A, Chang DT. Foreign body reaction to biomaterials. Semin Immunol. 2008; 20:86–100. [PubMed: 18162407]
2. Coleman DL, King RN, Andrade JD. The foreign body reaction: a chronic inflammatory response. J Biomed Mater Res. 1974; 8:199–211. [PubMed: 4609985]
3. Ratner BD, Bryant SJ. Biomaterials: where we have been and where we are going. Annu Rev Biomed Eng. 2004; 6:41–75. [PubMed: 15255762]
4. Klueh U, Kaur M, Qiao Y, Kreutzer DL. Critical role of tissue mast cells in controlling long-term glucose sensor function in vivo. Biomaterials. 2010; 31:4540–51. [PubMed: 20226521]
5. Anderson JM, Defife K, McNally A, Collier T, Jenney C. Monocyte, macrophage and foreign body giant cell interactions with molecularly engineered surfaces. J Mater Sci-Mater Med. 1999; 10:579–88. [PubMed: 15347970]
6. Ju YM, Yu BZ, Koob TJ, Moussy Y, Moussy F. A novel porous collagen scaffold around an implantable biosensor for improving biocompatibility. I. In vitro/in vivo stability of the scaffold and in vitro sensitivity of the glucose sensor with scaffold. J Biomed Mater Res Part A. 2008; 87A:136–46.
7. Ju YM, Yu BZ, West L, Moussy Y, Moussy F. A novel porous collagen scaffold around an implantable biosensor for improving biocompatibility. II. Long-term in vitro/in vivo sensitivity characteristics of sensors with NDGA- or GA-crosslinked collagen scaffolds. J Biomed Mater Res Part A. 2010; 92A:650–8.
8. Wang C, Yu B, Knudsen B, Harmon J, Moussy F, Moussy Y. Synthesis and performance of novel hydrogels coatings for implantable glucose sensors. Biomacromolecules. 2008; 9:561–7. [PubMed: 18166014]

9. Yu BZ, Wang CY, Ju YM, West L, Harmon J, Moussy Y, et al. Use of hydrogel coating to improve the performance of implanted glucose sensors. Biosens Bioelectron. 2008; 23:1278–84. [PubMed: 18182283]
10. Koh A, Nichols SP, Schoenfisch MH. Glucose sensor membranes for mitigating the foreign body response. J Diabetes Sci Technol. 2011; 5:1052–9. [PubMed: 22027297]
11. Ju YM, Yu BZ, West L, Moussy Y, Moussy F. A dexamethasone-loaded PLGA micirospheres/ collagen scaffold composite for implantable glucose sensors. J Biomed Mater Res Part A. 2010; 93A:200–10.
12. Ward WK, Wood MD, Casey HM, Quinn MJ, Federiuk IF. The effect of local subcutaneous delivery of vascular endothelial growth factor on the function of a chronically implanted amperometric glucose sensor. Diabetes Technol Ther. 2004; 19:155–63.
13. Patil SD, Papadmitrakopoulos F, Burgess DJ. Concurrent delivery of dexamethasone and VEGF for localized inflammation control and angiogenesis. J Control Release. 2007; 117:68–79. [PubMed: 17169457]
14. Norton LW, Koschwanez HE, Wisniewski NA, Klitzman B, Reichert WM. Vascular endothelial growth factor and dexamethasone release from non-fouling sensor coatings affect the foreign body response. J Biomed Mater Res Part A. 2007; 81A:858–69.
15. Edelman JL, Lutz D, Castro MR. Corticosteroids inhibit VEGF-induced vascular leakage in a rabbit model of blood-retinal and blood-aqueous barrier breakdown. Exp Eye Res. 2005; 80:249–58. [PubMed: 15670803]
16. Machein MR, Kullmer J, Ronicke V, Machein U, Krieg M, Damert A, et al. Differential downregulation of vascular endothelial growth factor by dexamethasone in normoxic and hypoxic rat glioma cells. Neuropathol Appl Neurobiol. 1999; 25:104–12. [PubMed: 10215998]
17. Thomassen MJ, Buhrow LT, Connors MJ, Kaneko FT, Erzurum SC, Kavuru MS. Nitric oxide inhibits inflammatory cytokine production by human alveolar macrophages. Am J Respir Cell Mol Biol. 1997; 17:279–83. [PubMed: 9308913]
18. Schwentker A, Vodovotz Y, Weller R, Billiar TR. Nitric oxide and wound repair: role of cytokines? Nitric Oxide-Biol Chem. 2002; 7:1–10.
19. Shukla A, Rasik AM, Shankar R. Nitric oxide inhibits wound collagen synthesis. Mol Cell Biochem. 1999; 200:27–33. [PubMed: 10569180]
20. Schäffer MR, Efron PA, Thornton FJ, Klingel K, Gross SS, Barbul A. Nitric oxide, an autocrine regulator of wound fibroblast synthetic function. J Immunol. 1997; 158:2375–81. [PubMed: 9036987]
21. Schäffer MR, Tantry U, Gross SS, Wasserkrug HL, Barbul A. Nitric oxide regulates wound healing. J Surg Res. 1996; 63:237–40. [PubMed: 8661204]
22. Thornton FJ, Schäffer MR, Witte MB, Moldawer LL, MacKay SLD, Abouhamze A, et al. Enhanced collagen accumulation following direct transfection of the inducible nitric oxide synthase gene in cutaneous wounds. Biochem Biophys Res Commun. 1998; 246:654–9. [PubMed: 9618268]
23. Cooke JP. NO and angiogenesis. Atheroscler Suppl. 2003; 4:53–60. [PubMed: 14664903]
24. Hetrick EM, Schoenfisch MH. Antibacterial nitric oxide-releasing xerogels: cell viability and parallel plate flow cell adhesion studies. Biomaterials. 2007; 28:1948–56. [PubMed: 17240444]
25. Hetrick EM, Prichard HL, Klitzman B, Schoenfisch MH. Reduced foreign body response at nitric oxide-releasing subcutaneous implants. Biomaterials. 2007; 28:4571–80. [PubMed: 17681598]
26. Nichols SP, Le NN, Klitzman B, Schoenfisch MH. Increased in vivo glucose recovery via nitric oxide release. Anal Chem. 2011; 83:1180–4. [PubMed: 21235247]
27. Gifford R, Batchelor MM, Lee Y, Gokulrangan G, Meyerhoff ME, Wilson GS. Mediation of in vivo glucose sensor inflammatory response via nitric oxide release. J Biomed Mater Res Part A. 2005; 75A:755–66.
28. Novak MT, Yuan F, Reichert WM. Modeling the relative impact of capsular tissue effects on implanted glucose sensor time lag and signal attenuation. Anal Bioanal Chem. 2010; 398:1695–705. [PubMed: 20803006]

29. Koh A, Riccio DA, Sun B, Carpenter AW, Nichols SP, Schoenfisch MH. Fabrication of nitric oxide-releasing polyurethane glucose sensor membranes. Biosens Bioelectron. 2011; 28:17–24. [PubMed: 21795038]
30. Sullivan TP, Eaglstein WH, Davis SC, Mertz P. The pig as a model for human wound healing. Wound Repair Regen. 2001; 9:66–76. [PubMed: 11350644]
31. Saavedra JE, Southan GJ, Davies KM, Lundell A, Markou C, Hanson SR, et al. Localizing antithrombotic and vasodilatory activity with a novel, ultrafast nitric oxide donor. J Med Chem. 1996; 39:4361–5. [PubMed: 8893830]
32. Shin JH, Metzger SK, Schoenfisch MH. Synthesis of nitric oxide-releasing silica nanoparticles. J Am Chem Soc. 2007; 129:4612–9. [PubMed: 17375919]
33. Riccio DA, Nugent JL, Schoenfisch MH. Stober synthesis of nitric oxide-releasing S-nitrosothiol-modified silica particles. Chem Mat. 2011; 23:1727–35.
34. Coneski PN, Schoenfisch MH. Nitric oxide release: part III. Measurement and reporting. Chem Soc Rev. 2012; 41:3753–8. [PubMed: 22362308]
35. Bancroft, J.; Gamble, M. Theory and practice of histological techniques. 6th. London: Churchill Livingstone; 2007.
36. Koschwanez HE, Yap FY, Klitzman B, Reichert WM. In vitro and in vivo characterization of porous poly-L-lactic acid coatings for subcutaneously implanted glucose sensors. J Biomed Mater Res Part A. 2008; 87A:792–807.
37. Davila JC, Lautsch EV, Palmer TE. Some physical factors affecting the acceptance of synthetic materials as tissue implants. Ann N Y Acad Sci. 1968; 146:138–47. [PubMed: 5238629]
38. Ward WK, Slobodzian EP, Tiekotter KL, Wood MD. The effect of micro-geometry, implant thickness and polyurethane chemistry on the foreign body response to subcutaneous implants. Biomaterials. 2002; 23:4185–92. [PubMed: 12194521]
39. Bota PCS, Collie AMB, Puolakkainen P, Vernon RB, Sage EH, Ratner BD, et al. Biomaterial topography alters healing in vivo and monocyte/macrophage activation in vitro. J Biomed Mater Res Part A. 2010; 95A:649–57.
40. Cao HQ, McHugh K, Chew SY, Anderson JM. The topographical effect of electrospun nanofibrous scaffolds on the in vivo and in vitro foreign body reaction. J Biomed Mater Res Part A. 2010; 93A:1151–9.
41. Barbe C, Bartlett J, Kong LG, Finnie K, Lin HQ, Larkin M, et al. Silica particles: a novel drug-delivery system. Adv Mater. 2004; 16:1959–66.
42. Hrabie JA, Keefer LK. Chemistry of the nitric oxide-releasing diazeniumdiolate ("nitrosohydroxylamine") functional group and its oxygen-substituted derivatives. Chem Rev. 2002; 102:1135–54. [PubMed: 11942789]
43. Davies KM, Wink DA, Saavedra JE, Keefer LK. Chemistry of the dia-zeniumdiolates. 2. Kinetics and mechanism of dissociation to nitric oxide in aqueous solution. J Am Chem Soc. 2001; 123:5473–81. [PubMed: 11389629]
44. Degraaf JC, Banga JD, Moncada S, Palmer RMJ, Degroot PG, Sixma JJ. Nitric oxide functions as an inhibitor of platelet adhesion under flow conditions. Circulation. 1992; 85:2284–90. [PubMed: 1591842]
45. Forstermann U. Nitric oxide and oxidative stress in vascular disease. Pflugers Arch. 2010; 459:923–39. [PubMed: 20306272]
46. Williams DLH. The chemistry of S-nitrosothiols. Acc Chem Res. 1999; 32:869–76.
47. Sieminski AL, Gooch KJ. Biomaterial-microvasculature interactions. Biomaterials. 2000; 21:2233–41.
48. Wisniewski N, Klitzman B, Miller B, Reichert WM. Decreased analyte transport through implanted membranes: differentiation of biofouling from tissue effects. J Biomed Mater Res. 2001; 57:513–21. [PubMed: 11553881]
49. Wilson GS, Gifford R. Biosensors for real-time in vivo measurements. Biosens Bioelectron. 2005; 20:2388–403. [PubMed: 15854814]
50. Jablecki M, Gough DA. Simulations of the frequency response of implantable glucose sensors. Anal Chem. 2000; 72:1853–9. [PubMed: 10784153]

51. Sharkawy AA, Klitzman B, Truskey GA, Reichert WM. Engineering the tissue which encapsulates subcutaneous implants. 1. Diffusion properties. J Biomed Mater Res. 1997; 37:401–12. [PubMed: 9368145]

52. Wisniewski N, Reichert M. Methods for reducing biosensor membrane biofouling. Colloid Surf B Biointerfaces. 2000; 18:197–219.

53. Gangjee T, Colaizzo R, Vonrecum AF. Species-related differences in percutaneous wound-healing. Ann Biomed Eng. 1985; 13:451–67. [PubMed: 4073629]

54. Wilson GS, Hu YB. Enzyme based biosensors for in vivo measurements. Chem Rev. 2000; 100:2693–704. [PubMed: 11749301]

55. Forster J, Morris AS, Shearer JD, Mastrofrancesco B, Inman KC, Lawler RG, et al. Glucose-uptake and flux through phosphofructokinase in wounded rat skeletal-muscle. Am J Physiol. 1989; 256:E788–97. [PubMed: 2525343]

56. Zhao QH, McNally AK, Rubin KR, Renier M, Wu Y, Rosecaprara V, et al. Human plasma alpha-2-macroglobulin promotes in vitro oxidative stress cracking of pellethane-2363-80A – in vivo and in vitro correlations. J Biomed Mater Res. 1993; 27:379–89. [PubMed: 7689567]

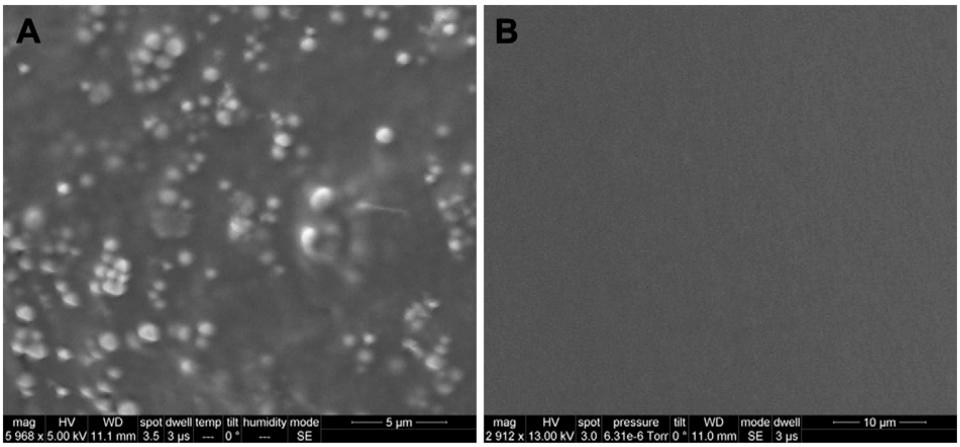

Fig. 1.

Scanning electron microscope images of polyurethane-coated wire substrates dipcoated four times in a polymer solution mixture of 36 mg/mL MPTMS nanoparticles and 80 mg/mL HPU/TPU A) before, and B) after topcoating with a 40 mg/mL HPU/TPU solution. Nanoparticle-induced surface roughness is masked after topcoating.

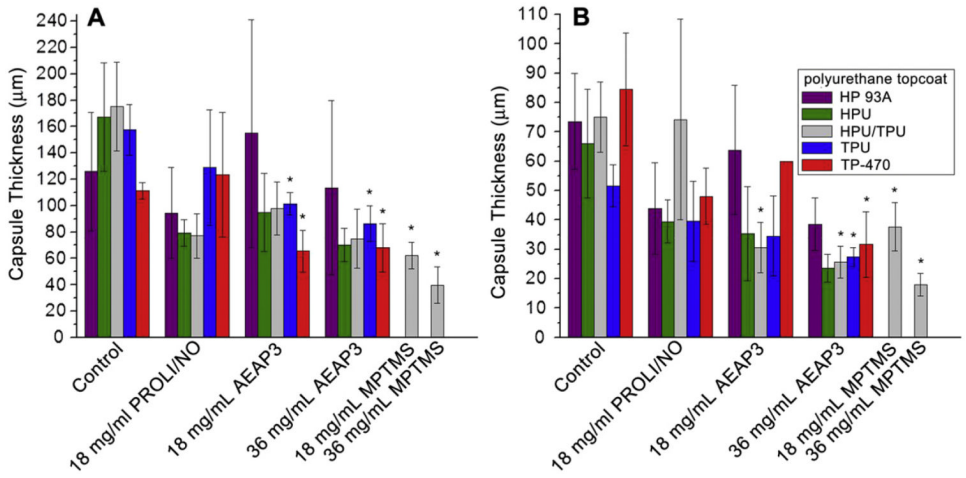

Fig. 2.

Collagen capsule thickness surrounding polyurethane-coated wire substrates at A) 3 and B) 6 weeks. Significant differences between NO-releasing and relative controls are indicated at $p < 0.05$ (*). At 6 weeks, the TP-470 topcoated 18 mg/mL AEAP3 nanoparticle system was not tested for statistical significance due to low sample size ($n = 2$).

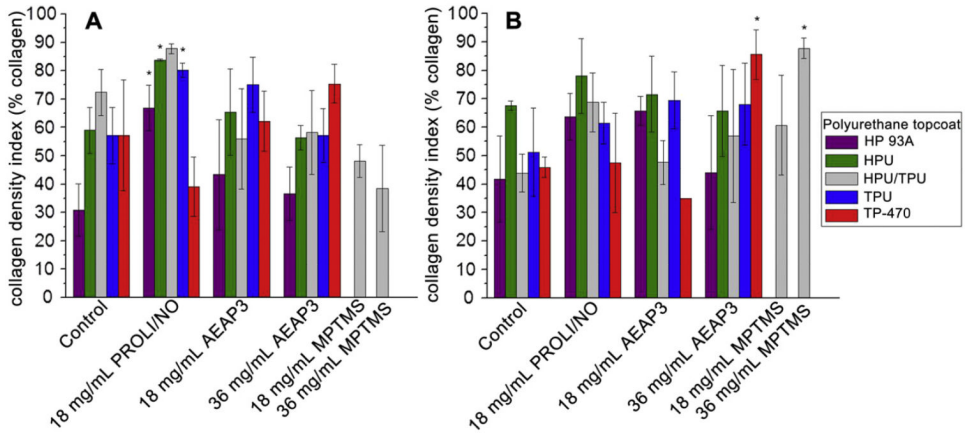

Fig. 3.

Collagen density index (CDI) of collagen capsules surrounding polyurethane-coated wire substrates at A) 3 and B) 6 weeks. Significant differences between NO-releasing and relative controls are indicated at $p < 0.05$ (*). At 6 weeks, the TP-470 topcoated 18 mg/mL AEAP3 nanoparticle system was not tested for statistical significance due to low sample size ($n = 2$).

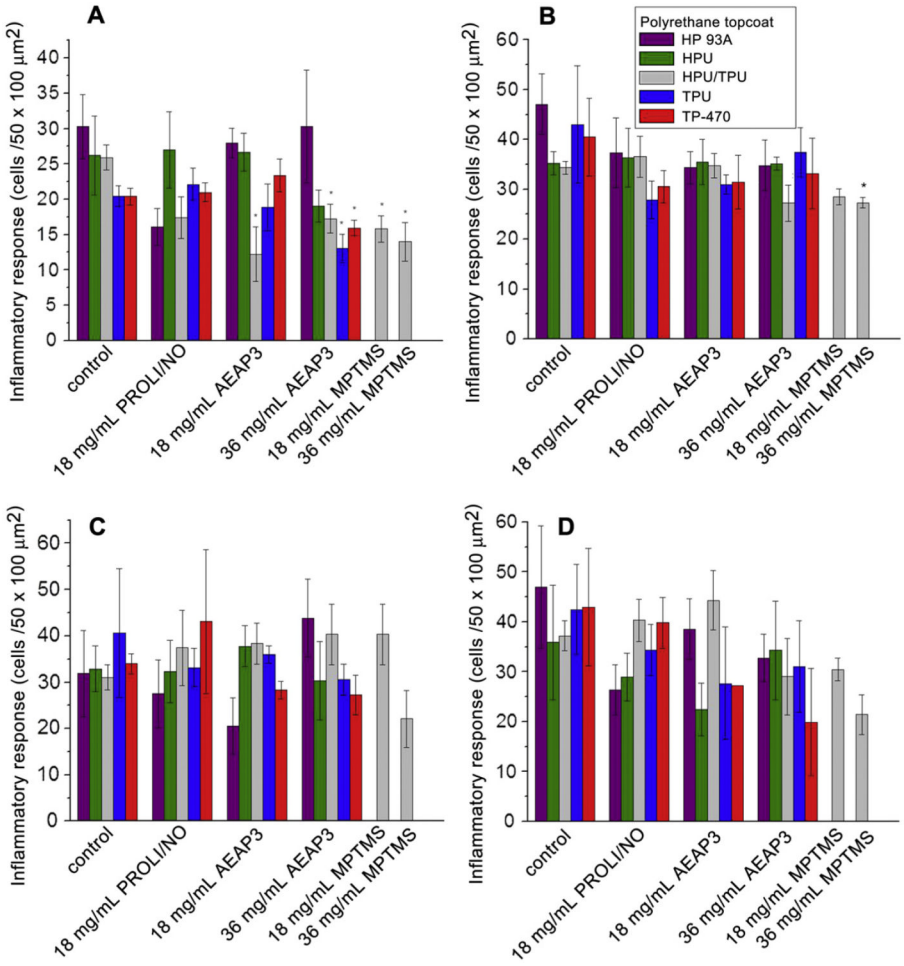

Fig. 4.

Inflammatory response to polyurethane-coated wire substrates at A) 3 d and B) 1, C) 3, and D) 6 weeks. Significant differences between NO-releasing and relative controls are indicated at $p < 0.05$ (*). At 6 weeks, the TP-470 topcoated 18 mg/mL AEAP3 nanoparticle system was not tested for statistical significance due to low sample size ($n = 2$).

Table 1

Water uptake of polyurethane topcoats [29].

Polyurethane	Water uptake (mg H_2O/mg PU)
Tecophilic HP-93A-100 (HP 93A)	2.56 ± 0.31
Hydrothane AL 25-80A (HPU)	0.63 ± 0.34
Tecoflex SG-80A (TPU)	0.20 ± 0.18
Tecoplast TP-470-000 (TP-470)	0.04 ± 0.05

Table 2

Nitric oxide release from coatings doped at 18 mg/mL PROLI/NO as a function of polyurethane topcoat.

NO release properties	Type of polyurethane topcoat				
	HP 93A	**HPU**	**HPU/TPU**	**TPU**	**TP-470**
$[NO]_{max}$ (pmol cm^{-2} s^{-1})	3128 ± 716	2895 ± 435	2617 ± 395	1526 ± 234	1436 ± 261
t_{max} (min)	8.4 ± 0.8	8.4 ± 0.6	9.1 ± 0.5	18.0 ±1.2	16.8 ± 2.5
$[NO]_{6\,h}$ (pmol cm^{-2} s^{-1})	5.45 ± 2.38	6.72 ± 2.19	23.47 ± 3.91	28.49 ± 3.69	26.53 ± 4.45
$[NO]_{12\,h}$ (pmol cm^{-2} s^{-1})	0	1.85 ± 0.23	2.54 ± 0.36	5.67 ± 0.71	6.89 ± 0.80
$[NO]_{24\,h}$ (pmol cm^{-2} s^{-1})	0	0	0.94 ± 0.32	1.67 ± 0.30	1.96 ± 0.26
Total NO (μmol cm^{-2})	3.9 ± 0.4	3.8 ± 0.5	4.1 ± 0.5	4.2 ± 0.5	4.1 ± 0.4

Table 3

Nitric oxide release from coatings doped at 18 mg/mL AEAP3 nanoparticles as a function of polyurethane topcoat.

NO release properties	Type of polyurethane topcoat				
	HP 93A	**HPU**	**HPU/TPU**	**TPU**	**TP-470**
$[NO]_{max}$(pmol cm $^{-2}$ s $^{-1}$)	108.8 ± 23.6	102.3 ± 19.8	99.66 ± 22.32	76.51 ± 21.55	41.78 ± 9.13
t_{max} (min)	9.2 ± 1.0	7.2 ± 1.1	19.2 ± 3.0	66 ± 16	84 ± 20
$[NO]_{6\,h}$ (pmol cm^{-2} s^{-1})	28.04 ± 4.21	49.57 ± 5.16	45.36 ± 4.84	42.82 ± 5.76	38.26 ± 8.31
$[NO]_{12\,h}$ (pmol cm^{-2} s^{-1})	10.94 ± 1.94	19.37 ± 2.62	21.29 ± 2.39	18.54 ± 1.62	21.59 ± 4.19
$[NO]_{24\,h}$ (pmol cm^{-2} s^{-1})	1.02 ± 0.31	1.86 ± 0.24	2.28 ± 0.31	5.61 ± 0.96	10.67 ± 2.47
$[NO]_{48\,h}$ (pmol cm^{-2} s^{-1})	0	0.98 ± 0.04	1.13 ± 0.08	1.37 ± 0.09	1.74 ± 0.21
Total NO (μmol cm^{-2})	2.7 ± 0.3	3.0 ± 0.3	3.0 ± 0.4	2.8 ± 0.3	2.7 ± 0.3

Table 4

Nitric oxide release from coatings doped at 36 mg/mL AEAP3 nanoparticles as a function of polyurethane topcoat.

NO release properties	Type of polyurethane topcoat				
	HP 93A	**HPU**	**HPU/TPU**	**TPU**	**TP-470**
$[NO]_{max}$ (pmol cm $^{-2}$ s^{-1})	353.6 ± 87.9	324.2 ± 68.2	316.1 ± 71.3	189.2 ± 51.4	123.4 ± 36.1
t_{max} (min)	7.2 ± 0.9	6.6 ± 0.8	18.0 ± 2.8	72 ± 19	96 ± 21
$[NO]_{6\,h}$ (pmol cm^{-2} s^{-1})	84.65 ± 10.61	92.95 ± 8.95	111.11 ± 13.51	68.18 ± 7.12	86.79 ± 6.94
$[NO]_{12\,h}$ (pmol cm^{-2} s^{-1})	30.28 ± 4.12	35.88 ± 3.32	38.93 ± 3.16	41.56 ± 3.56	51.54 ± 5.84
$[NO]_{24\,h}$ (pmol cm^{-2} s^{-1})	2.80 ± 0.71	3.64 ± 0.42	5.12 ± 1.02	10.05 ± 1.80	10.91 ± 1.11
$[NO]_{48\,h}$ (pmol cm $^{-2}$ s $^{-1}$)	0.96 ±0.17	1.12 ± 0.06	1.35 ± 0.31	2.58 ± 0.64	2.84 ± 0.43
$[NO]_{72\,h}$ (pmol cm $^{-2}$ s^{-1})	0	0.92 ± 0.04	1.15 ± 0.16	1.28 ± 0.08	1.56 ±0.17
Total NO (μmol cm^{-2})	6.1 ± 0.6	6.1 ± 0.5	6.0 ± 0.5	5.9 ± 0.6	5.8 ± 0.5

Table 5

Nitric oxide release from coatings doped at 18 mg/mL or 36 mg/mL MPTMS nano-particles with a HPU/TPU polyurethane topcoat.

NO release properties	Nanoparticle concentration doped into polyurethane	
	18 mg/mL	36 mg/mL
$[NO]_{max}$ (pmol cm $^{-2}$ s $^{-1}$)	287.3 ± 19.7	383.9 ± 32.9
t_{max} (min)	9.0 ±1.6	9.1 ± 2.2
$[NO]_{6\,h}$ (pmol cm^{-2} s^{-1})	31.73 ± 2.23	73.51 ± 6.62
$[NO]_{12\,h}$ (pmol cm^{-2} s^{-1})	14.2 ± 1.56	31.16 ± 2.91
$[NO]_{24h}$ (pmol cm^{-2} s^{-1})	6.78 ± 0.62	12.58 ± 1.34
[NO] (pmol cm^{-2} s^{-1})	2.69 ± 0.34	5.18 ± 0.41
[NO] (pmol cm^{-2} s^{-1})	1.59 ± 0.12	1.67 ± 0.10
[NO]14 d (pmol cm^{-2} s^{-1})	1.06 ± 0.12	1.29 ± 0.13
Total NO (μmol cm $^{-2)}$	5.1 ± 0.4	9.3 ± 0.6